A SUPERSONIC TUNNEL FOR LASER AND FLOW-SEEDING TECHNIQUES

Robert J. Bruckner
National Aeronautics and Space Administration
Lewis Research Center
Cleveland, Ohio 44135

and

Jan Lepicovsky
NYMA, Inc.
Engineering Services Division
Brook Park, Ohio 44142

Abstract

A supersonic wind tunnel with flow conditions of 3 lbm/s (1.5 kg/s) at a free-stream Mach number of 2.5 was designed and tested to provide an arena for future development work on laser measurement and flow-seeding techniques. The hybrid supersonic nozzle design that was used incorporated the rapid expansion method of propulsive nozzles while it maintained the uniform, disturbance-free flow required in supersonic wind tunnels. A viscous analysis was performed on the tunnel to determine the boundary layer growth characteristics along the flowpath. Appropriate corrections were then made to the contour of the nozzle. Axial pressure distributions were measured and Mach number distributions were calculated based on three independent data reduction methods. A complete uncertainty analysis was performed on the precision error of each method. Complex shock-wave patterns were generated in the flow field by wedges mounted near the roof and floor of the tunnel. The most stable shock structure was determined experimentally by the use of a focusing schlieren system and a novel, laser-based dynamic shock position sensor. Three potential measurement regions for future laser and flow-seeding studies were created in the shock structure: (1) deceleration through an oblique shock wave of 50°, (2) strong deceleration through a normal shock wave, and (3) acceleration through a supersonic expansion fan containing 25° of flow turning.

Nomenclature

A	cross-sectional area, in.^{2} (mm^2)
B	bias component of uncertainty
g	boundary layer form parameter (δ^*/δ)
l	length of subsonic contractions, in. (mm)
M	Mach number
n	boundary layer power profile parameter
P	pressure, psia (kPa)
PR	precision component of uncertainty
S	tunnel blockage parameter
U	measurement uncertainty
W	width of the flowpath, in. (mm)
x	subsonic contraction abscissa, in. (mm)
Y	convergent/divergent nozzle ordinate, in. (mm)
ΔY	correction factor for boundary layer mass flow defect, in. (mm)
y	subsonic contraction ordinate, in. (mm)
γ	ratio of specific heats of an ideal gas
δ	boundary layer thickness, in. (mm)
δ^*	boundary layer displacement thickness, in. (mm)

Subscripts:

a	total-static Mach number calculation method
b	Pitot-total Mach number calculation method
c	Pitot-static Mach number calculation method
e	exit conditions
i	subsonic inlet condition

p Pitot conditions

s static conditions

t total conditions

Superscript:

$*$ throat/sonic conditions

Introduction

A supersonic wind tunnel was designed and constructed at the NASA Lewis Research Center for fundamental laser velocimetry (LV) and flow-seeding techniques in complex high-speed flows. Additional experience with these techniques applied to complex flow regimes was necessary to interpret the data obtained from flow-seeding techniques. The consequences of particle lag, dynamic velocity response, and condensation effects of flow-seeding techniques need to be better understood and quantified to be properly applied to complex supersonic flows. Information relating to these effects can only be attained through experimentation on the measurement system. Therefore, a known flow condition must be used to compare the laser and flow-seeding technique responses to the actual flow field conditions. Previous experiments of this nature only examined LV measurements through oblique shock waves or unsteady bow shocks.[1,2] Both types of experiments have limitations, making it difficult to extract quantitative information relating the response of the given technique to actual flow conditions. For the oblique shock, the limitation was the change in flow direction as well as the magnitude of velocity; for the bow shocks, the limitation was the unsteadiness of the normal shock front and the presence of a body in the desired measurement region.

The objectives of the work described herein were to design a supersonic wind tunnel with a maximum-length constant-Mach-number region and to develop a spatially and temporally stable shock wave pattern. The first of these objectives was constrained by the overall facility test section length; therefore, a hybrid nozzle design approach was applied using the rapid expansion method of propulsive nozzles and maintained the uniform, disturbance-free flow required in supersonic wind tunnels. The use of this approach resulted in the length of the constant Mach number region being maximized at 21 in. (533 mm), which was greater than 65 percent of the length available for the entire test section. Additionally, the viscous effect of boundary layer growth along the supersonic flowpath was calculated, and appropriate corrections were made to the coordinates of the contoured nozzle walls.

The second objective was achieved by utilizing the stability of attached, oblique shock waves generated by supersonic wedge flow and shock wave interaction to create complex flow conditions. Complex shock wave patterns were generated by wedges mounted near the roof and floor of the tunnel. These wedges were traversed into the Mach-2.5 flow by a pair of linear actuators.

Conventional aerodynamic instrumentation was incorporated in the tunnel to completely specify the high-speed complex flow field independent of laser and flow-seeding measurement techniques. The tunnel was instrumented to measure inlet total temperature and pressure, exit diffuser static pressure, and nozzle wall static pressure distribution. A three-element total pressure rake was used to perform axial Pitot pressure surveys of the core flow. Mach numbers were calculated using three different data reduction equations; physical assumptions and measurement uncertainties were analyzed for each equation.

Two flow visualization methods were utilized to identify and quantify the shock structure stability. A focusing schlieren system was designed and constructed to provide flow visualization of the baseline nozzle flow and shock wave patterns. A novel laser-based dynamic position sensor was used to accurately map the shock structure and to determine the spatial amplitude of the shock unsteadiness.

Aerodynamic Design

Subsonic Contractions

To limit the maximum test section flow rate to 3 lbm/s (1.5 kg/s), the sonic throat area for this tunnel was set at 1.4 in.^{2} (36 mm^2). Since the facility designed for this test section contained a plenum with an exit opening of 6 in.^{2} (152 mm^2), two subsonic contraction sections were needed to achieve this design condition. The first contraction section transformed the square bellmouth exit to a rectangular 36- by 152-mm flow. The second contraction section transformed the rectangular flow to the desired square sonic flow. A diagram of the supersonic tunnel has been included in Fig. 1. The design of these contractions was based on the inviscid, compressible subsonic nozzle theory of Vitoshinski.[3] The nondimensional contour equation and a figure describing the nomenclature are presented in Eq. (1) and Fig. 2, respectively.

$$y = \frac{y_e}{\left\{1-\left[1-\left(\frac{y_e}{y_i}\right)^2\right]\frac{\left[1-\left(\frac{x}{l}\right)^2\right]^2}{\left[1+\frac{1}{3}\left(\frac{x}{l}\right)^2\right]^3}\right\}^{0.5}} \tag{1}$$

Supersonic Region

For computational convenience, the supersonic region of the nozzle was divided into three sections: expansion,

flow-straightening, and constant-Mach-number. The expansion and flow-straightening sections were designed according to the two-dimensional method of characteristics.[4,5]

The basic principle of supersonic wind tunnel design is twofold. Primarily, the effective area ratio must be achieved such that the flow reaches the desired Mach number. Second, the wall contours must allow all wave disturbances which originate from the expansion section to be geometrically eliminated in the flow-straightening section, yielding a purely one-dimensional flow at the exit. The assumptions used in the calculations of the preliminary nozzle contour in these sections were

(1) Inviscid, irrotational flow
(2) Ideal gas behavior
(3) One-dimensional sonic flow at the throat
(4) Zero-thickness expansion waves

A computer code was written to expedite this design phase and to provide more accuracy in the calculations. A more detailed description of this program is contained in Ref. 6.

Boundary Layer Corrections

Viscous boundary layer corrections to the contoured nozzle block coordinates were performed to compensate for the mass flow deficit of the displacement thickness. After the inviscid nozzle contour design was complete, a boundary layer analysis was performed on the supersonic region. The boundary layer thickness at the throat was assumed to be zero because of the favorable pressure gradient up to the sonic line.[7] The remainder of the viscous analysis followed the method and theory outlined by Tucker.[8,9] This method was chosen primarily for two reasons: (1) its use to model the flow in a gas dynamically and geometrically similar supersonic wind tunnel; (2) the ease of the calculations required to obtain the desired results.[10] A complete derivation of this method and definition of the various quantities are documented in the literature.[9] These quantities were tabulated by Tucker as functions of both Mach number and boundary layer profile parameter {f(M,n)}; polynomial curve fits were generated to simplify the design computations.[8]

Once the boundary layer growth along the supersonic region was calculated, the displacement thickness was calculated using form parameter $g = \delta^*/\delta$.[9] Throughout these calculations, a one-seventh power profile was assumed to be the turbulent boundary layer shape based on Sibulkin's measurements.[11] Ultimately, the displacement thickness growth on all four tunnel walls was converted to an equivalent adjustment of only the two symmetrical nozzle blocks by

$$\Delta Y = \delta^* \left[1 + \left(\frac{Y_{cp}}{W} \right) - \left(\frac{2\delta^*}{W} \right) \right] \qquad (2)$$

Figure 3 demonstrates the physical parameters used in Eq. (2). Figure 4 compares the convergent/divergent (C/D) supersonic nozzle contour based on viscous and inviscid calculations.

Shock-Wave-Generating Hardware

To fulfill the final aerodynamic requirement of this supersonic LV calibration tunnel, a method was designed to establish a normal shock wave in the constant-Mach-number section. Two methods that were considered were (1) increased diffuser pressure once supersonic flow is established and (2) a mechanical system taking advantage of supersonic wedge flow principles. Because of the inherent instabilities of precise pressure regulation and its associated effects on the shock structure, the first method was ruled out. The method used to generate the complex shock waves utilized the stability of attached oblique waves and shock wave interaction to achieve the desired result. The leading edges of these wedges were elevated above the wall boundary layer of the tunnel and the width was reduced to avoid any detrimental interaction effects on the shock-wave boundary layer. Linear actuators and variable wedge angle inserts were used to experimentally determine the optimum shock-generating hardware configuration. Photographs of the shock-generating hardware are shown in Figs. 5 and 6.

Experimental Setup

Facility Interfaces

The supersonic tunnel was designed for a continuous-flow aeronautics facility.[12] The facility was equipped with a plenum which has an internal volume of 35.3 ft^3 (1 m^3) and an exit bellmouth, which provided uniform two-dimensional flow through a 6-in.^{2} (152-mm^2) opening. The contraction ratio for this bellmouth is 28:1. Maximum inlet flow rates, total pressure, and temperature limits for this facility are 10 lbm/s (4.6 kg/s), 55 psia (379 kPa), and 810 R (450 K), respectively. The minimum sustainable backpressure for this facility is 1.5 psia (10 kPa). The size of the diffuser exhaust flange is limited to 6 in.^{2} (152 mm^2) and the overall available test section length is limited to 32 in. (813 mm).

Instrumentation Setup

The C/D nozzle and the walls of the constant-Mach-number section were instrumented with 0.020-in.-(0.51-mm) diameter static pressure orifices along the vertical centerline of the tunnel. These orifices were installed normal to the flow surface to within 0.10°. The axial locations of the orifices were accurate within 0.005 in. (0.13 mm) and are tabulated in Table 1. Total pressure and temperature probes were located in the plenum chamber upstream from the test section. Static pressure was measured in the 6-in.^{2} (152-mm^2) diffuser section located downstream from the test section. Pitot pressure surveys were conducted using the three-element total pressure rake shown in Fig. 7. These surveys spanned the final 4 in. (100 mm) of the test section upstream from the exit plane. Temperatures were measured

by Chromel-Alumel thermocouples connected to a commercial temperature measurement system.[13] Static and total pressures were connected to a high-accuracy electronic differential pressure scanning system coupled with a digital barometer.[14]

Focusing Schlieren System

A focusing schlieren system was designed and constructed for this experiment according to the description of Weinstein[15] and is a modern adaptation of the original design proposed by Burton.[16] The system obtained qualitative flow visualization of the nozzle flow and shock wave patterns formed in the test section. The major advantage of the focusing schlieren system over the conventional system is its ability to visualize density gradients in one plane while keeping disturbances outside of the region of interest out of focus. The sensitivity of the system was equal in both the horizontal and vertical directions.

Shock Position Sensor

A novel laser-based shock position sensor was used to accurately map the complex shock structure of the flow field.[17] This technique used the beam diffraction phenomenon observed when a laser beam intersects a shock front at a grazing angle.

Results

Analytic

Axial Mach number distributions were calculated along the entire length of the C/D nozzle and constant-Mach-number section. The subsonic parameters were calculated using the isentropic, compressible-gas-dynamic formulas.[18] Using the coordinates of the subsonic contractions and an assumed sonic area of 1.4 in.^{2} (36 mm^2) the free-stream Mach number was determined by

$$\frac{A}{A^*}=\left[\frac{2}{\gamma+1}\right]^{\gamma+1/2(\gamma-1)}\left[\frac{1}{M}\right]\left[1+\left(\frac{\gamma-1}{2}\right)M^2\right]^{-\gamma+1/2(\gamma-1)} \tag{3}$$

Supersonic parameters were also calculated with Eq. (3) using the contour points generated by the inviscid design program as input. Additionally, axial Mach number distributions were calculated along the nozzle wall and tunnel centerline based on two-dimensional theory. Results of these distributions are included with the experimental results of Figs. 8(a) and (b).

Data Reduction and Uncertainty Analysis

Three methods were used to calculate Mach number distributions based on measurements of plenum, static, and Pitot pressures, P_t, P_s, and P_p, respectively. The following equations were used:

$$\frac{P_s}{P_t}=\left[1+\left(\frac{\gamma-1}{2}\right)M_a^2\right]^{\gamma/\gamma-1} \tag{4}$$

$$\frac{P_p}{P_t}=\left[\frac{(\gamma+1)M_b^2}{(\gamma-1)M_b^2+2}\right]^{\gamma/\gamma-1}\left[\frac{\gamma+1}{2\gamma M_b-(\gamma-1)}\right]^{1/\gamma-1} \tag{5}$$

$$\frac{P_p}{P_s}=\left[\frac{(\gamma+1)M_c^2}{2}\right]^{\gamma/\gamma-1}\left[\frac{\gamma+1}{2\gamma M_c-(\gamma-1)}\right]^{1/\gamma-1} \tag{6}$$

An uncertainty analysis was performed on each method to verify the accuracy of the Mach number distribution of this supersonic tunnel. The analysis followed the procedures outlined by the Advisory Group for Aeronautical Research and Development (AGARD).[19] The total measurement error was assumed to be a root-mean-square combination of bias and precision components (Eq. (7)).

$$U=\sqrt{PR^2+B^2} \tag{7}$$

Bias components were those effects which result in systematic errors such as zero shifts in transducers, leakage of the pressure measurement tubing, oversized or nonorthogonal static orifices, and probe misalignments. Precision components result in random errors stemming primarily from instrumentation and transducer inaccuracy.

For the purposes of this analysis, it was assumed that the bias error component was negligible because proper instrumentation designs were used for the static pressure taps and total pressure probes as well as on-line, in situ calibrations of the pressure transducers.[20,21] Precision limits for the independent pressure measurements were determined through documented accuracies of the pressure transducers and instrumentation designs.[13,14] An estimate of the precision error component was then made by calculating the partial derivative of the Mach number with respect to the independent parameters according to

$$PR=\sqrt{\sum_{i=1}^{J}\left[\left(\frac{\partial M}{\partial P_i}\right)P_i\right]^2} \tag{8}$$

Uncertainty error components for the various Mach number calculation methods were calculated based on Eqs. (9) to (10). A summary of the measurement uncertainties has been included in Table 1.

$$U_a = \frac{1+\left(\frac{\gamma-1}{2}\right)M_a^2}{\gamma M_a}\left[\left(\frac{dP_t}{P_t}+\frac{dP_s}{p_s}\right)^2\right]^{0.5} \quad (9)$$

$$U_b = \frac{-(\gamma-1)\left[M_b^2+\frac{2}{\gamma-1}\right]\left[2\gamma M_b^2-(\gamma-1)\right]}{4\gamma\left(M_b^2-1\right)^2}$$

$$\times\left[\left(\frac{dP_t}{P_t}\right)^2+\left(\frac{dP_p}{P_p}\right)^2\right]^{0.5} \quad (10)$$

Experimental Baseline Aerodynamics

Experiments were performed on the C/D nozzle only (without shock-generating hardware installed) to obtain the baseline performance of the tunnel. The test conditions are summarized in Table 2.

Mach number distributions that were calculated based on all three methods are presented in Figs. 8 to 10. These figures were generated based on isentropic flow conditions throughout the tunnel. Both one- and two-dimensional theories have been included in Fig. 8 for comparison.

Complex Shock Structure

Complex shock-wave patterns were created by the specially designed hardware and actuator systems described in the Shock-Wave-Generating Hardware Section and shown in Figs. 5 and 6. The optimum configuration was determined experimentally (Fig. 11). This shock structure was established by two wedges; the forward wedge had an angle of 25.3° relative to the flow and the aft wedge had an angle of 12.3°. The wedges were separated by 1.66 in. (42.2 mm) in height and were axially offset by 1.25 in. (31.8 mm). Schlieren photographs of the flow field around the wedges are included in Fig. 12. Also shown in these photographs is the sensitivity of the shock structure when the forward wedge is moved ±0.200 in. (±5 mm) from the nominal, most stable position. The resulting shock structure provided three potential measurement regions for the laser and flow-seeding studies: (1) deceleration through an oblique shock wave, (2) strong deceleration through a normal shock wave, and (3) acceleration though an expansion fan. The stability of the shock waves was determined by a dynamic shock position instrument. The preliminary results of these studies indicated a maximum spatial amplitude of the normal shock wave unsteadiness of ±0.016 in. (±0.4 mm).

Discussion

The proposed supersonic tunnel design method has proven to be an effective procedure for maximizing the constant Mach number region while maintaining uniform flow through the tunnel. However, Fig. 8 indicated that the flow decelerated slightly through the Mach-2.5 region. This deceleration is a result of several factors, including errors in the calculation of displacement thickness, errors in the correction of the C/D nozzle contour coordinates, and three-dimensional effects of the boundary layers on the side walls and corners. Without detailed knowledge of the flow field in the freestream and boundary layers, any attempt to correct this deceleration would be unscientific. Also seen in the baseline aerodynamics of the tunnel is a lower free-stream Mach number, based on the total-static method, for higher total pressures and Reynold's numbers. Two possible reasons for this lower free-stream Mach number are leakage of air between the total pressure measurement point and the test section or a thicker boundary layer at higher pressures as a result of the elevated Reynold's number.

Trends in the Mach number distributions based on the Pitot-total and Pitot-static methods appear to be random. No conclusions can be drawn from these data. The existence of a bias error on the Pitot pressure measurement is also possible because the rake was not calibrated prior to testing. However, the bias would be expected to be much smaller than the precision error because of its size and proper flow alignment. An implied assumption of both the total-static and Pitot-total methods was that the total pressure measured in the plenum remained constant throughout the tunnel, based on the relative magnitude of the viscous effects calculated in the boundary layer analysis. However, the consistency of the Mach number distribution based on the Pitot-static method, which did not rely on this assumption, verifies the validity of that assumption.

The goal of successfully developing a complex shock structure in the tunnel was also achieved. Schlieren flow visualization and dynamic shock position studies indicated that the experimentally determined shock structure was very stable in steady-state operation and in tunnel startup. This stability has eliminated the need for actuators in the tunnel to position the wedges after supersonic flow has been established. Critical development experience for the shock-generating hardware resulted in reducing the width of the wedges to eliminate the shock-wave-boundary layer interaction along the sidewalls and on the roof and floor of the tunnel. The reduction of the overall thickness of the wedges to avoid tunnel unstart problems caused by blockage and second throat effects also resulted. Figure 13, which includes data from the present experiment and from Ref. 7, proved to be very useful in the determination of the maximum allowable tunnel blockage.

Summary

The hybrid supersonic nozzle design was highly successful in obtaining a maximum constant Mach number region with excellent flow quality. The viscous flow analysis

was sufficient to obtain the desired results. Improvements to this algorithm would require detailed knowledge of the three-dimensional velocity profiles which was beyond the scope of this work. The complex shock structure generated in this tunnel was very robust and stable under all operating conditions including tunnel startup. The need for the wedge system actuation was eliminated by the reduction in the wedge frontal area. The spatial stability of the individual shock waves was ±0.016 in. (±0.4 mm). Three potential measurement regions were created in the complex shock wave pattern. These measurement regions included a deceleration through a normal shock, an oblique shock, and an acceleration through an expansion fan. Extensive experimental investigations are now possible in the optimum laser and flow-seeding techniques that are required to make non-intrusive velocity measurements in complex supersonic flows.

References

1. Resinger, D., Heiser, W., Olejak, D., and Wagner, S., "Investigation of a Plate-Ramp-Configuration by Means of Laser Doppler Anemometry at Different Mach Numbers," AIAA Paper 92–3956, July 1992.
2. Michel, F., D'Hummeres, C., and Papirnyk O., "Aerosol Behavior in Supersonic Flows," Laser Anemometry Advances and Applications—Part 3, ASME, 1991.
3. Vitoshinski, C., "Uber Strahlerweiterung und Strahlablenkung," In: Th. von Karman und T. Levi-Civita (Heraugeber): Vortrage aus dem Gebeit der Hydro- und Aerodynamik, (Innsbruck 1922), pp. 248–251, Julius Springer, Berlin 1924.
4. Anderson Jr., J.D., Modern Compressible Flow with Historical Perspective, McGraw-Hill, Inc., New York, 1982.
5. Kuethe, A.M., and Chow, C-Y., Foundations of Aerodynamics, John Wiley & Sons, Inc., New York, 1986.
6. Bruckner, R.J., "Design and Aerodynamic Performance of a Supersonic Laser Velocimetry Calibration Tunnel," Master's Thesis, Cleveland State University, Cleveland, OH., 1993.
7. Pope, A., and Goin, K.L., High-Speed Wind Tunnel Testing, John Wiley & Sons, Inc., New York, 1965.
8. Tucker, M., "Approximate Turbulent Boundary-Layer Development In Plane Compressible Flow Along Thermally Insulated Surfaces With Application to Supersonic-Tunnel Contour Correction," NACA TN 2045, 1950.
9. Tucker, M., "Approximate Calculation of Turbulent Boundary-Layer Development in Compressible Flow," NACA TN 2337, 1951.
10. Brinich, P.F., "Boundary-Layer Measurements in 3.84- by 10- Inch Supersonic Channel," NACA TN 2203, 1950.
11. Sibulkin, M., "Boundary-Layer Measurements at Supersonic Nozzle Throats," Journal of the Aeronautical Sciences, pp. 249–252, 264, Ap. 1957.
12. Bruckner, R.J., Buggele, A.E., and Lepicovsky, J., "Engine Component Instrumentation Development Facility at NASA Lewis Research Center," AIAA Paper 92–3995, July 1992.
13. Omega Technologies Co., The Temperature Handbook, 1989.
14. Hyscan 2000 pressure measurement system manual, Scanivalve Inc., 1990.
15. Weinstein, L.M., "An Improved Large Field Focussing Schlieren System," AIAA Paper 91–0567, 1991.
16. Burton, R.A., "A Modified Schlieren Apparatus for Large Areas of Field," J. Opt. Sc. Am. Vol. 39, Nov. 1949, pp. 907–908.
17. Panda, J., "Partial Spreading of a Laser Beam into a Light Sheet by Shock Waves and its use as a Shock Detection Technique," NASA CR–195329, 1994.
18. "Equations, Tables, and Charts for Compressible Flow," NACA Report 1135, 1953.
19. Advisory Group for Aerospace Research and Development, "Assessment of Wind Tunnel Measurement Uncertainty," AGARD–AR–304, 1987.
20. Shaw, R., "The Influence of Hole Dimension on Static Pressure Measurements," Journal of Fluid Mechanic, Vol. 7, pp. 550–564, 1960.
21. Leipmann, H.W., and Roshko, A., Elements of Gasdynamics, John Wiley & Sons, Inc., New York 1957.

TABLE 1.—SUMMARY OF INSTRUMENTATION LOCATION AND MEASUREMENTS UNCERTAINTIES

[Total pressure, P_t = 25.5 psia (175.9 kPa).]

Pressure orifice	Axial location, in. (mm)	Pressure range, ±psia (±kPa)	Pressure error, psia (kPa)	Mach number, M_a	Measurement uncertainty, U_a
Method a					
P_{s1}	−0.25 (−6.35)	15 (103.5)	0.00955 (0.0659)	0.947	0.00127
P_{s2}	1.25 (31.75)	15 (103.5)	0.01150 (0.0793)	1.830	0.00193
P_{s3}	2.75 (69.85)	15 (103.5)	0.01172 (0.0808)	2.020	0.00248
P_{s4}	4.25 (107.95)	15 (103.5)	0.01188 (0.0819)	2.208	0.00328
P_{s5}	5.75 (146.05)	15 (103.5)	0.01199 (0.0827)	2.364	0.00417
P_{s6}	6.75 (171.45)	15 (103.5)	0.01203 (0.0830)	2.438	0.00469
P_{s7}	7.28 (184.95)	15 (103.5)	0.01205 (0.0831)	2.486	0.00506
P_{s8}	9.25 (234.95)	15 (103.5)	0.01204 (0.0831)	2.468	0.00492
P_{s9}	10.25 (260.35)	5 (34.5)	0.03844 (0.2652)	2.454	0.01515
P_{s10}	11.25 (285.75)	5 (34.5)	0.03845 (0.2652)	2.460	0.01531
P_{s11}	12.25 (311.15)	5 (34.5)	0.03844 (0.2652)	2.456	0.01521
P_{s12}	14.25 (361.95)	5 (34.5)	0.03843 (0.2651)	2.428	0.01455
P_{s13}	17.25 (438.15)	5 (34.5)	0.03842 (0.2650)	2.419	0.01433
P_{s14}	20.25 (514.35)	5 (34.5)	0.03843 (0.2651)	2.426	0.01450
P_{s15}	22.25 (565.15)	5 (34.5)	0.03842 (0.2650)	2.413	0.01420
P_{s16}	25.25 (641.35)	5 (34.5)	0.03841 (0.2650)	2.394	0.01378

Pressure orifice	Axial location, in. (mm)	Pressure range, psia, (kPa)	Pressure error, psia, (kPa)	Mach number, M_b	Measurement uncertainty, U_b	Mach number, M_c	Measurement uncertainty, U_c
Method b,c							
P_t	plenum	50 (345)	0.33 (2.3)	--------	--------	-------	----------
P_p	21.3–25.2 (541–641)	50 (345)	0.31 (2.1)	2.411	0.0013	2.387	0.0063

TABLE 2.—CONDITIONS FOR THE BASELINE PERFORMANCE TESTS

Reynold's number, 1/ft (1/m)	$2.4–8.9\times10^6$ ($0.72–2.71\times10^6$)
Total pressure, psia (kPa)	10.8, 14.6, 25.9, 40.4 (74.5, 100.7, 178.7, 278.7)
Total temperature, R (K)	519 (288)
Dew point, R (K)	440 (244)
Minimum pressure, psia (kPa)	1.25 (8.6)

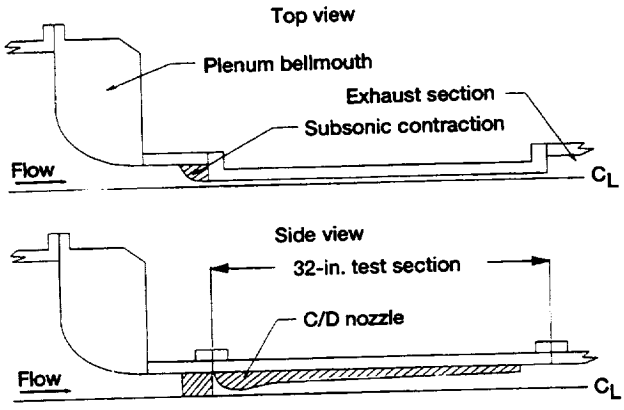

Figure 1.—Supersonic tunnel including shock-generating hardware.

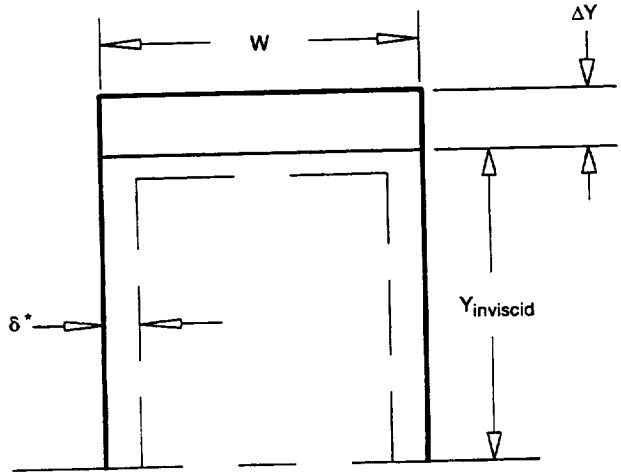

Figure 3.—Two-dimensional contour correction based on three-dimensional boundary layer growth.

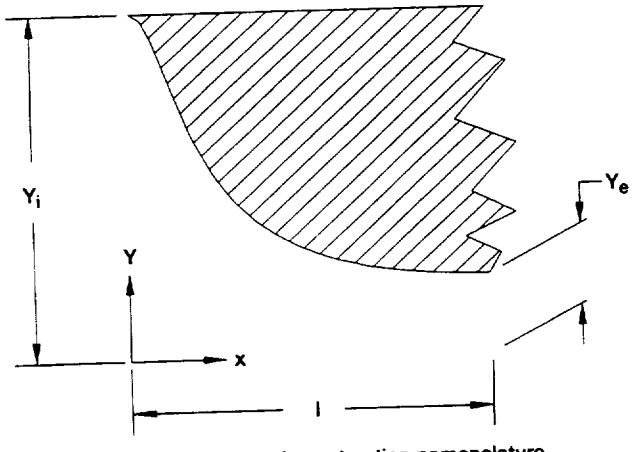

Figure 2.—Subsonic contraction nomenclature.

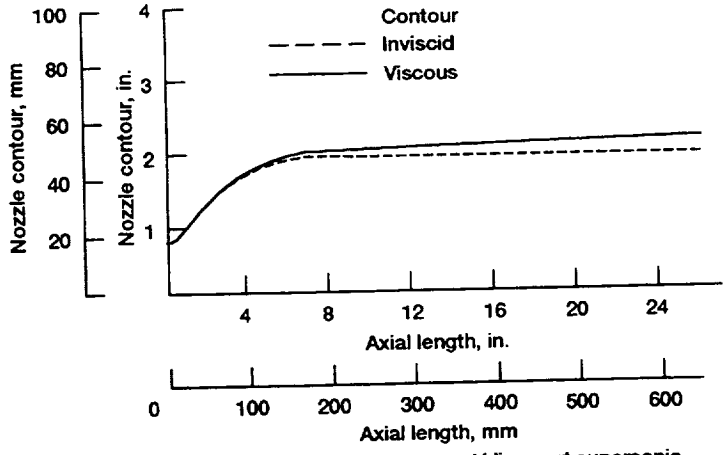

Figure 4.—Comparison of convergent/divergent supersonic nozzle countour based on viscous and inviscid analysis.

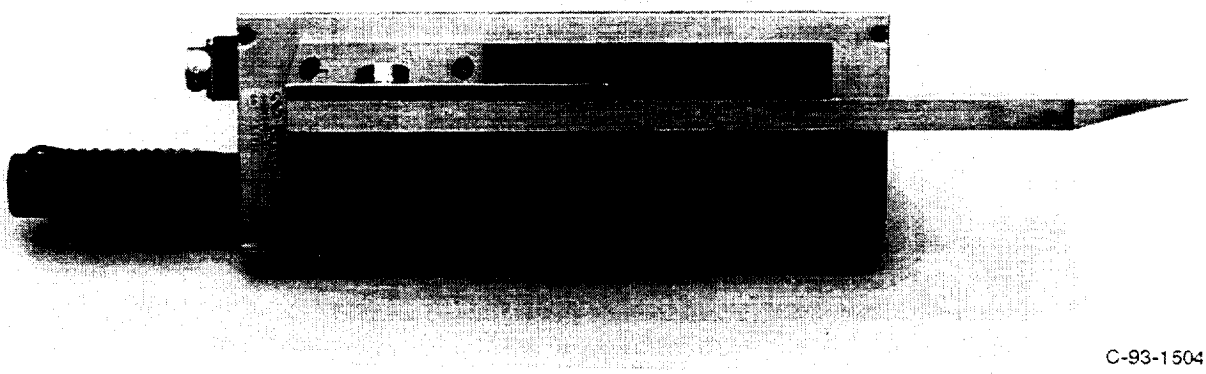

C-93-1504

Figure 5.—Shock-generating hardware mounted on linear actuator.

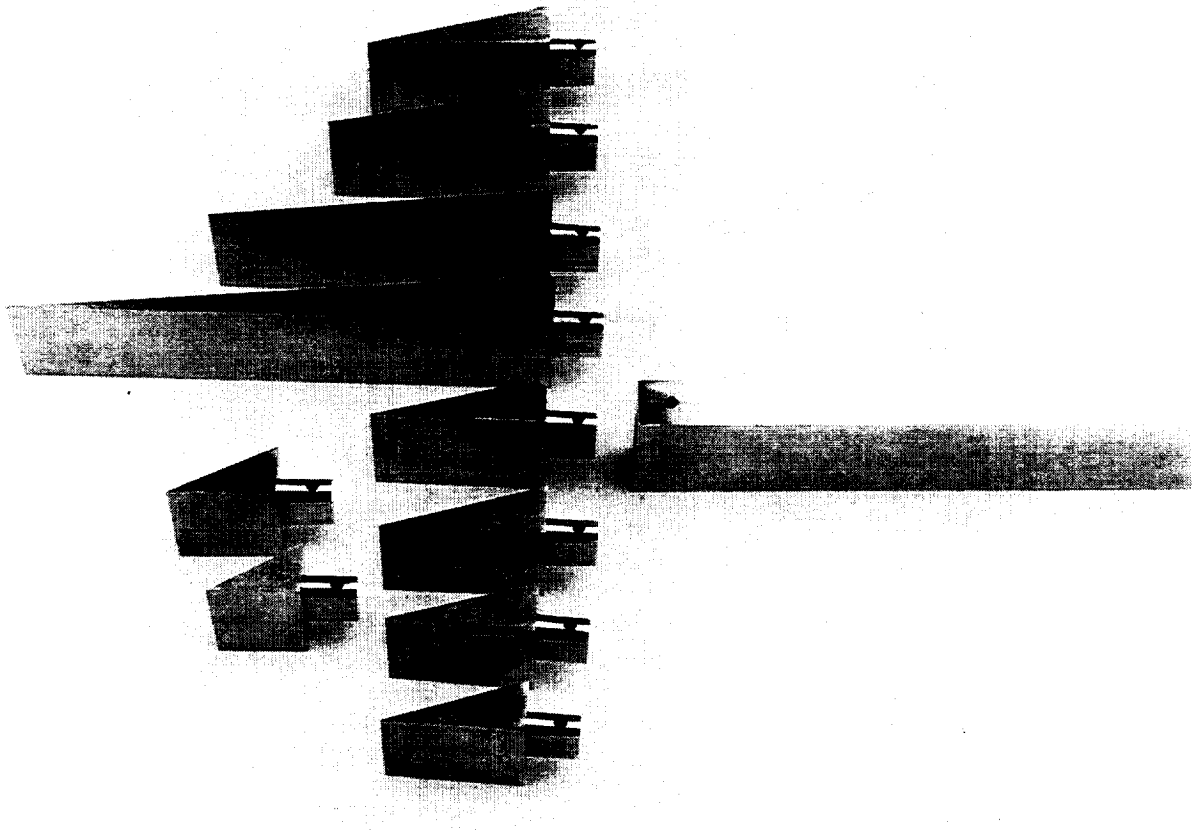

C-93-1506

Figure 6.—Shock-generating hardware showing all available wedge angles.

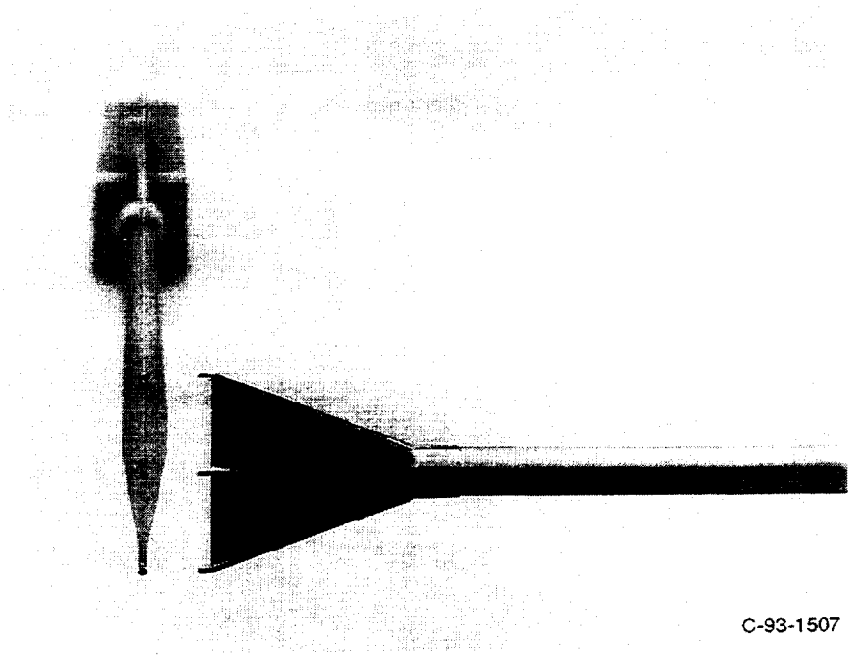

Figure 7.—Three-element total pressure Pitot rake.

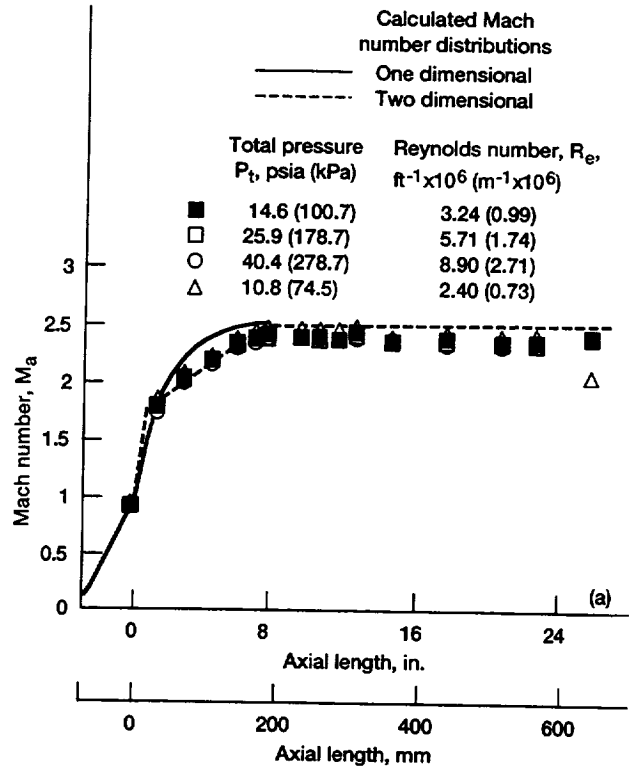

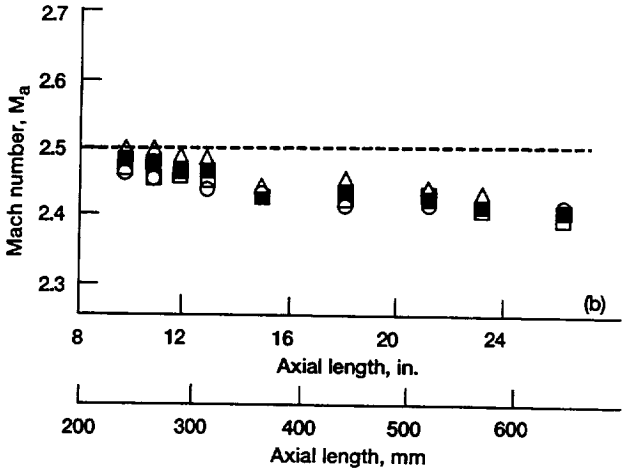

Figure 8.—Experimental Mach number distributions for various Reynold's numbers based on total-static method. (a) Entire test section. (b) Mach number section.

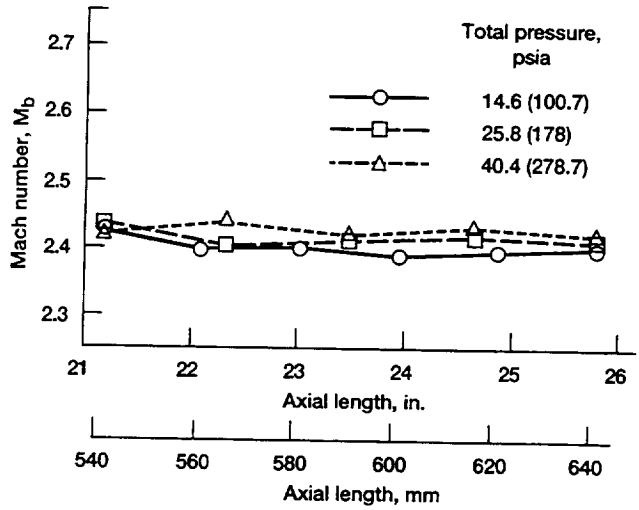

Figure 9.—Experimental Mach number distribution based on Pitot-total method.

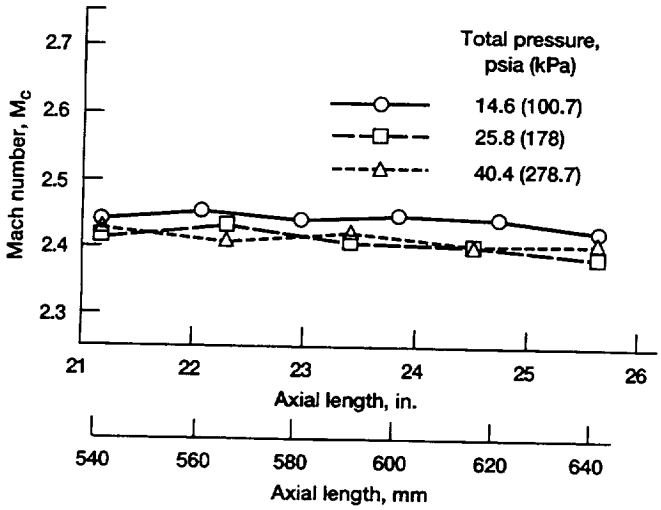

Figure 10.—Experimental Mach number distribution based on Pitot-static method.

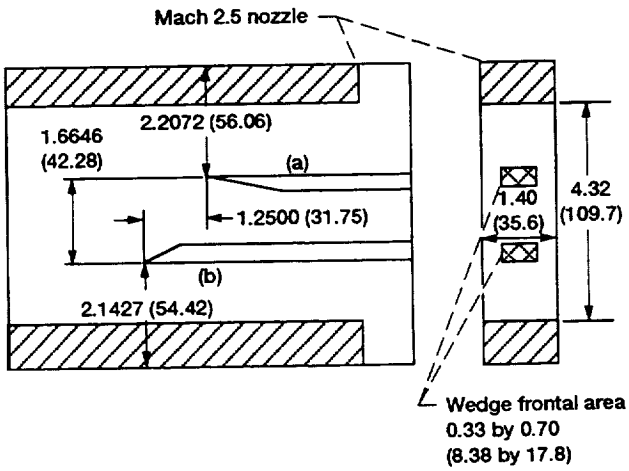

Figure 11.—Optimum shock-generating hardware. (a) 12.3°. (b) 25.3°. Dimensions are in inches (mm).

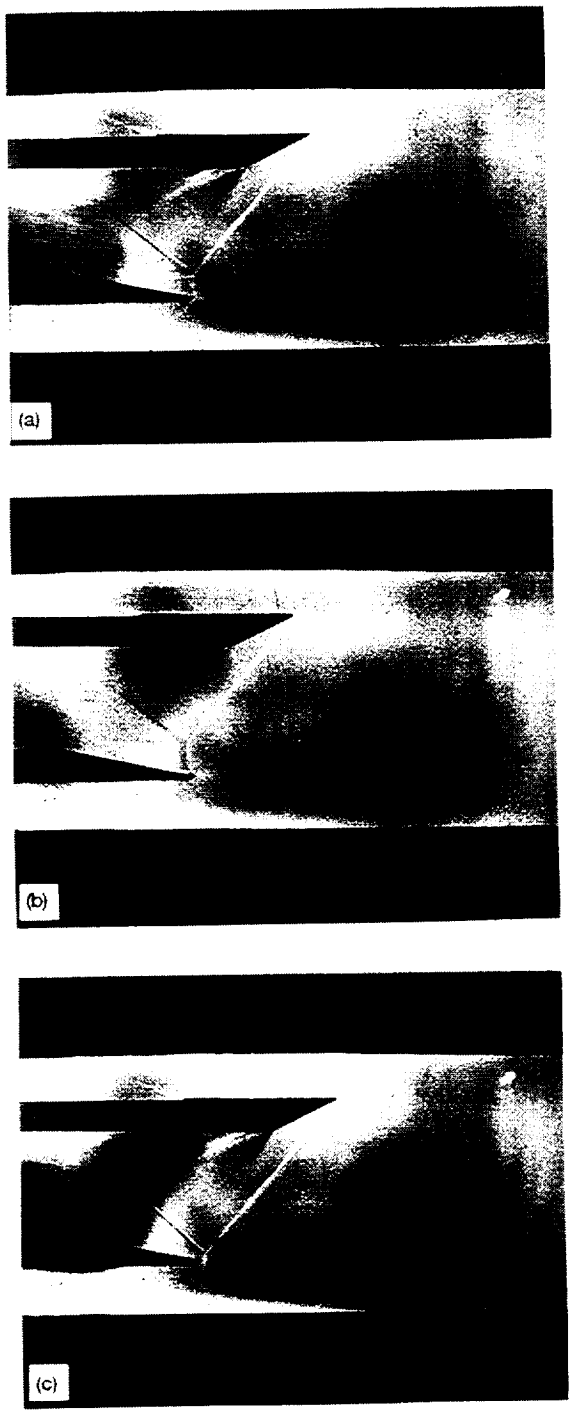

Figure 12.—Schlieren photograph of shock structure. (a) Nominal position. (b) +0.200 in. (+5 mm). (c) –0.200 in. (–5 mm).

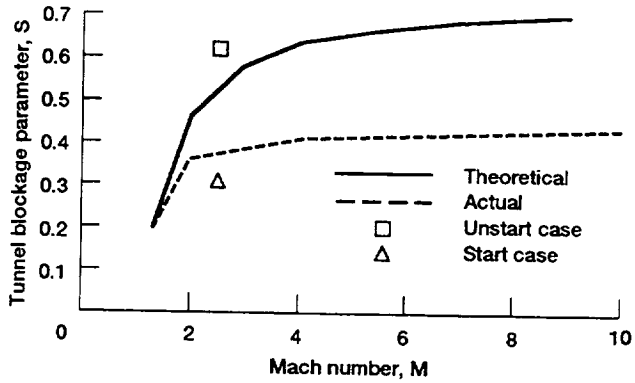

Figure 13.—Maximum allowable blockage of supersonic tunnel versus Mach number. Blockage parameter S defined as mean model diameter divided by square root of inviscid tunnel cross-sectional area.

REPORT DOCUMENTATION PAGE

Form Approved
OMB No. 0704-0188

Public reporting burden for this collection of information is estimated to average 1 hour per response, including the time for reviewing instructions, searching existing data sources, gathering and maintaining the data needed, and completing and reviewing the collection of information. Send comments regarding this burden estimate or any other aspect of this collection of information, including suggestions for reducing this burden, to Washington Headquarters Services, Directorate for Information Operations and Reports, 1215 Jefferson Davis Highway, Suite 1204, Arlington, VA 22202-4302, and to the Office of Management and Budget, Paperwork Reduction Project (0704-0188), Washington, DC 20503.

1. AGENCY USE ONLY (*Leave blank*)	2. REPORT DATE	3. REPORT TYPE AND DATES COVERED
	June 1994	Technical Memorandum

4. TITLE AND SUBTITLE

A Supersonic Tunnel for Laser and Flow-Seeding Techniques

5. FUNDING NUMBERS

WU–505–62–10

6. AUTHOR(S)

Robert J. Bruckner and Jan Lepicovsky

7. PERFORMING ORGANIZATION NAME(S) AND ADDRESS(ES)

National Aeronautics and Space Administration
Lewis Research Center
Cleveland, Ohio 44135–3191

8. PERFORMING ORGANIZATION REPORT NUMBER

E–8852

9. SPONSORING/MONITORING AGENCY NAME(S) AND ADDRESS(ES)

National Aeronautics and Space Administration
Washington, D.C. 20546–0001

10. SPONSORING/MONITORING AGENCY REPORT NUMBER

NASA TM–106588
AIAA–94–1825

11. SUPPLEMENTARY NOTES

Prepared for the 12th Applied Aerodynamics Conference sponsored by the American Institute of Aeronautics and Astronautics, Colorado Springs, Colorado, June 20–24, 1994. Robert J. Bruckner, NASA Lewis Research Center; and Jan Lepicovsky, NYMA, Inc., Engineering Services Division, 2001 Aerospace Parkway, Brook Park, Ohio 44142 (work funded by NASA Contract NAS3–27186). Responsible person, Robert J. Bruckner, organization code 2840, (216) 433–6499.

12a. DISTRIBUTION/AVAILABILITY STATEMENT

Unclassified - Unlimited
Subject Category 34

12b. DISTRIBUTION CODE

13. ABSTRACT ***(Maximum 200 words)***

A supersonic tunnel with flow conditions of 3 lbm/s (1.5 kg/s) at a free-stream Mach number of 2.5 was designed and tested to provide an arena for future development work on laser measurement and flow-seeding techniques. The hybrid supersonic nozzle design that was used incorporated the rapid expansion method of propulsive nozzles while it maintained the uniform, disturbance-free flow required in wind tunnels. A viscous analysis was performed on the tunnel to determine the boundary layer growth characteristics along the flowpath. Appropriate corrections were then made to the contour of the nozzle. Axial pressure distributions were measured and Mach number distributions were calculated based on three independent data reduction methods. A complete uncertainty analysis was performed on the precision error of each method. Complex shock-wave patterns were generated in the flow field by wedges mounted near the roof and floor of the tunnel. The most stable shock structure was determined experimentally by the use of a focusing schlieren system and a novel, laser-based dynamic shock position sensor. Three potential measurement regions for future laser and flow-seeding studies were created in the shock structure: (1) deceleration through an oblique shock wave of 50°, (2) strong deceleration through a normal shock wave, and (3) acceleration through a supersonic expansion fan containing 25° of flow turning.

14. SUBJECT TERMS

Supersonic wind tunnel; Measurement uncertainty; Schlieren flow visualization

15. NUMBER OF PAGES

15

16. PRICE CODE

A03

17. SECURITY CLASSIFICATION OF REPORT	18. SECURITY CLASSIFICATION OF THIS PAGE	19. SECURITY CLASSIFICATION OF ABSTRACT	20. LIMITATION OF ABSTRACT
Unclassified	Unclassified	Unclassified	